

Direct-Conversion Flat-Panel X-Ray Image Sensors for Digital Radiography

SAFA O. KASAP, SENIOR MEMBER, IEEE, AND JOHN A. ROWLANDS

Invited Paper

Advances in active-matrix array flat panels for displays over the last decade have lead to the development of flat-panel X-ray image detectors. Recent flat-panel detectors have shown image quality exceeding that of X-ray film/screen cassettes. They can also permit the instantaneous capture, readout, and display of digital X-ray images and, hence, enable the clinical transition to digital radiography. There are two general approaches to flat panel detector technology: 1) direct and 2) indirect conversion. The present paper outlines the operating principles for direct-conversion detectors based on the use of photoconductors. It formulates and reviews the required X-ray photoconductor properties for such applications and examines to what extent potential materials fulfill these requirements. The quantum efficiency, X-ray sensitivity, noise, and detective quantum efficiency factors are discussed with reference to current and potential large area X-ray photoconductors.

Keywords—Direct-conversion detector, flat panel, sensor, X-ray image detector.

I. PRINCIPLES OF THE DIRECT-CONVERSION DIGITAL X-RAY IMAGE DETECTOR

If a radiologist were to speculate about the ideal X-ray imaging system, what might come to mind is a digital flat-panel system that is able to perform all clinically important radiographic techniques at reduced dose. It would, immediately after the patient's X-ray exposure, provide a high-quality radiograph on a video monitor and would also be usable for real-time imaging (e.g., fluoroscopy). The physical form of the system would be similar to a film/screen cassette so that it would easily fit into current medical X-ray systems. Indeed, the connection from the detector to the

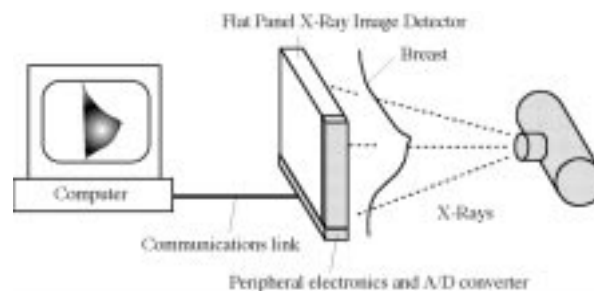


Fig. 1. Schematic illustration of a flat-panel X-ray image detector for digital mammography. Connection from the detector to a local or distant computer is a convenient communications link (e.g., a wireless link allowing a more versatile detector usage).

imaging system may be a wireless link, making the detector more portable, versatile, and easier to use. Such a system would record an X-ray image directly on to a computer, rapidly display it and allow it to be analyzed with image processing techniques, as shown in Fig. 1. Today, 65% of medical X-ray imaging is still film-based analog technology. This laborious process can take several minutes during which time the patient has to remain undressed and the X-ray room is engaged. However, digital radiography has started to make inroads.

At present, essentially two methods have been adopted for digital radiography. Both are based on the use of phosphors, i.e., both involve indirect conversion from an X-ray photon to a detectable charge signal [1]. The first is the digitization of a signal from a video camera optically coupled to an X-ray image intensifier (cesium iodide phosphor). The second is the photostimulable phosphor system [commonly called computed radiography (CR) system] that captures a latent image within a storage phosphor layer, which is subsequently readout with a laser scanner. Of these, the intensifier system permits instant readout, but is very bulky while the CR system, like film/screen, requires carrying the cassette from a loading/unloading station to the patient examination room and back. Neither of these indirect-conversion

Manuscript received April 23, 2001; revised November 11, 2002. This work was supported by the Natural Sciences and Engineering Research Council of Canada and the National Cancer Institute of Canada under a Terry Fox Program Project Grant "Imaging for Cancer."

S. O. Kasap is with the Department of Electrical Engineering, University of Saskatchewan, Saskatoon, SK S7N 5A9, Canada (e-mail: Safa_Kasap@Engr.usask.ca).

J. A. Rowlands is with the Departments of Medical Imaging and Medical Biophysics, University of Toronto, Toronto, ON M4N 3N5, Canada (e-mail: john.rowlands@swchsc.on.ca).

Publisher Item Identifier S 0018-9219(02)03959-2.



Fig. 2. Flat-panel active-matrix direct-conversion X-ray imager using a-Se as the X-ray to charge transducer with an active area of 14×17 in. (Courtesy of the Direct Radiography Corporation.)

phosphor-based systems has adequate image quality for all applications. The need for a digital radiography system that reads out images electronically and directly and with better image quality remains.

Recent research has identified flat-panel digital radiographic systems based on a large-area thin-film transistor (TFT) active-matrix array (AMA) used in flat-panel displays as a promising readout technique. This approach permits essentially instantaneous readout and higher quality than is possible with previous methods. One approach uses an electroded X-ray photoconductor [2], as shown in Fig. 2. The key factor in flat-panel X-ray detector technology was the development of TFT arrays that matured as the fabrication and doping of large area hydrogenated amorphous-silicon (a-Si:H) films became technologically possible in the early 1990s [3]. This development was primarily directed at the consumer application to displays. However, the requirements for an AMA for a detector are essentially identical and so X-ray detectors are a useful spinoff. The combination of an AMA and an X-ray photoconductor constitutes a direct-conversion X-ray image detector. The term direct conversion refers to the fact that the X-ray photons are directly converted to charges that are subsequently collected. This is to be contrasted with indirect-conversion systems, where there is an intermediate conversion, via a phosphor, to photons (light) and then from photons to charge [4], [5].

For both indirect- and direct-conversion approaches, the latent image is a charge distribution residing on the panel's pixels. The charges simply are read out by scanning the arrays row by row using the peripheral electronics and multiplexing the parallel columns to a serial digital signal as illustrated in Fig. 3. This signal is then transmitted to a computer system. The system is simple, inherently digital, and has so many advantages that it has now become a major contender in digital radiography (e.g., [2], [6]–[8]).

An AMA, as depicted in Fig. 3, consists of millions of individual pixel electrodes connected by TFTs (one for each pixel) to electrodes passing over the whole array to subsidiary electronics on the periphery. The TFTs act as switches to control the clocking out of image charge a line at a time. Very large area (e.g., $40 \text{ cm} \times 40 \text{ cm}$) AMAs are now

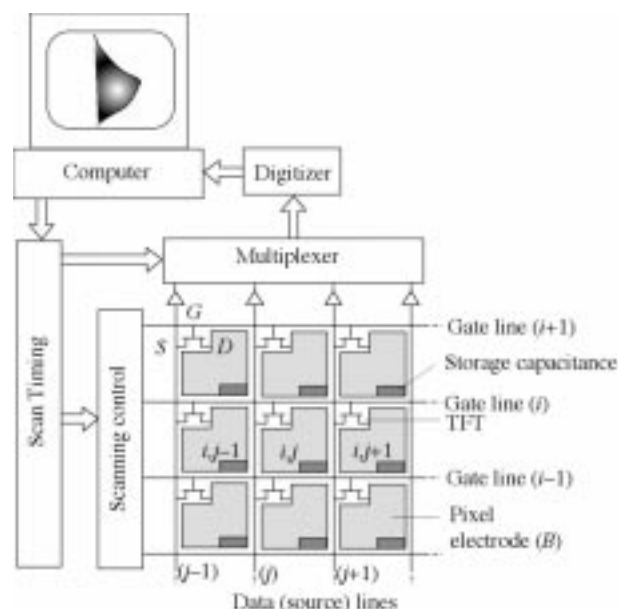


Fig. 3. TFT AMA for use in X-ray image detectors with self-scanned electronic readout. Charge distribution residing on the panel's pixels are simply readout by scanning the arrays row by row using the peripheral electronics multiplexing the parallel columns to a serial digital signal.

becoming available and even larger ones should be possible in the future. The AMA consists of $M \times N$ (e.g., 2480×3072) storage capacitor C_{ij} , whose charge can be read through addressing the TFT (i, j) via the gate (i) and source (j) lines. An external readout electronics and software, by self-scanning, converts the charges read on each C_{ij} to a digital image as explained below. Self-scanning here refers to the fact that no external means, such as a scanning laser beam as in some other digital X-ray imaging systems, is used to scan the pixels and extract the information. The scanning operation is part of the flat-panel detector electronics and its software and occurs across the image plane permitting a truly compact device.

Research and development into both indirect and direct-conversion flat-panel imagers is ongoing and only time will tell which is the most suitable for each imaging modality. However, our research has identified the direct-conversion method as possibly the highest resolution approach and probably the most economic to manufacture due to the simplicity of the AMA panel structure and ease with which the X-ray photoconductor can be integrated with it.

In direct-conversion detectors, a layer of semiconductor such as stabilized a-Se is coated onto the AMA to serve as an X-ray photoconductor, as shown in Fig. 4. An electrode (labeled A) is subsequently deposited on the a-Se layer to enable the application of a biasing potential and, hence, an electric field F in the a-Se layer. The applied bias voltage to the radiation receiving electrode A may be positive or negative, the selection of which is discussed below. With negative bias on A , the electron hole pairs (EHPs) that are generated in the photoconductor by the absorption of an X-ray photon travel along the field lines. Holes are collected by the positive bias electrode (A) and electrons accumulate on the storage

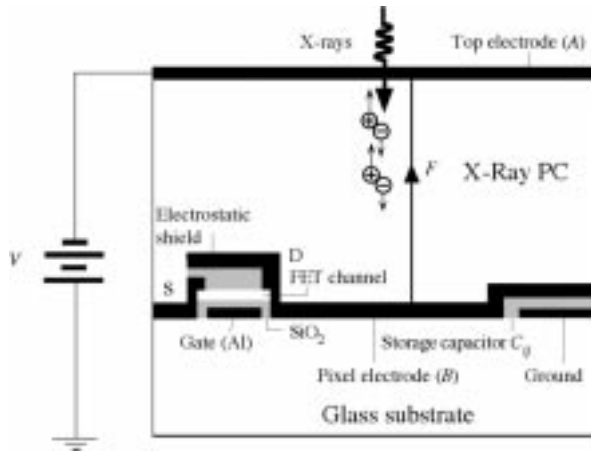


Fig. 4. Highly simplified cross section of a single pixel (i, j) with a TFT showing the accumulation of X-ray generated charge on the pixel electrode and, hence, the storage capacitance C_{ij} . The top electrode (A) on the photoconductor is a vacuum coated metal (e.g., Al). The bottom electrode (B) is the pixel electrode that is one of the plates of the storage capacitance (C_{ij}). (Not to scale and the FET height is highly exaggerated.)

capacitor C_{ij} and, thereby, provide a charge signal ΔQ_{ij} that can be read during self-scanning. Each pixel electrode carries an amount of charge ΔQ_{ij} that is proportional to the amount of incident X-ray radiation by virtue of the X-ray photoconductivity of the photoconductor over that pixel. The equivalent circuit of a single pixel is shown in Fig. 5. The X-ray generated charge ΔQ_{ij} is collected and stored on the storage capacitance C_{st} . The FET is switched on every Δt seconds to read this charge on the pixel via a charge amplifier. The applied bias is typically several kilovolts for an a-Se-based photoconductor and can be positive or negative. The negative bias shown on the receiving electrode in Fig. 5 has the advantage that the device is self-protecting to high-voltage damage. For example, if a quantity of radiation beyond the normal operational conditions is incident on the detector, a very large charge can accumulate on the pixel electrode and, hence, the voltage on C_{st} can rise to potentially damaging levels. (Typically, the TFT has a breakdown voltage of ~ 50 V, whereas the applied bias is several kilovolts.) However, as negative voltage builds up on the pixel electrode due to exposure, a voltage is reached that partially turns on the FET and removes the charge before it can build up further to a level where breakdown of the FET could occur causing permanent damage. In the case of positive bias, the photoconductor-pixel design has to be modified to prevent breakdown either by using a dielectric layer between the bias electrode A and a-Se or by incorporating additional switching elements into the pixel to bleed off excess charge.

To facilitate the readout of the latent image, all TFTs in a row have their gates connected, whereas all TFTs in a column have their sources connected. When gate line i is activated, all TFTs in that row are turned “on” and N data lines (from $j = 1$ to N) read the charges on the pixel electrodes in row i . The parallel data are multiplexed into serial data, digitized, then fed into a computer for imaging. The scanning control activates the next row $i + 1$ and all the pixel charges

in this row are read and multiplexed, until the whole matrix has been read from the first to the last row (M th row). Fig. 6 shows an X-ray image of a skull phantom obtained by a flat-panel X-ray image detector using an a-Se X-ray photoconductor at a clinically acceptable radiation dose level. The resolution is primarily determined by the pixel size which in present experimental image detectors is typically $100\text{--}150\ \mu\text{m}$, but could be as small as $50\ \mu\text{m}$ in future high-resolution detectors for mammography. An interesting feature of the a-Se-based flat-panel X-ray sensor is that this technology has been made possible by the use of two key elemental amorphous semiconductors: a-Si:H and amorphous selenium (a-Se). Although their properties are different, both can be readily prepared in large areas, which is essential for an X-ray image detector. It will be impracticably difficult and expensive to develop a large-area detector using a single crystal technology.

Any flat-panel X-ray image detector design must first consider the required specifications based on the clinical need of the particular imaging modality, e.g., mammography, chest radiology, and fluoroscopy.

Table 1 summarizes the specifications for flat-panel detectors for chest radiology, mammography, and fluoroscopy. The quoted noise level is the quantum noise of the minimum radiation to which the panel will be exposed.

II. INTRINSIC RESOLUTION OF X-RAY PHOTOCONDUCTORS

Photoconductors that directly convert the X-ray radiation to EHPs have a number of distinct advantages, one of which is their intrinsic high resolution. The resolution of an imaging device or a system is specified in terms of its modulation transfer function (MTF), which is the relative response of the system as a function of spatial frequencies and is discussed later in this review. The higher the MTF, the better the resolution can be. It is instructive to examine the intrinsic resolution of a photoconductor-based detector. Consider an electroded a-Se layer that has been biased to establish a field F in the photoconductor and assume that the pixel size is negligible small. X-rays absorbed in the photoconductor release EHPs. Holes are drawn to the top electrode and become neutralized; electrons accumulate on the storage capacitance C_{st} , so forming the latent charge image.

The lateral spreading of information and, hence, the loss of resolution in a photoconductor-based detection system can be attributed to a number of causes. Que and Rowlands [9] in 1995 evaluated the intrinsic spatial resolution of an a-Se photoconductor. The extension of these ideas to the present electroded system suggests the following causes for the loss of resolution:

- 1) the range of primary electrons generated by the photoelectric effect;
- 2) reabsorption of characteristic K-fluorescent X-rays away from the original photoelectric absorption site;
- 3) reabsorption of Compton scattered photons;
- 4) lateral diffusion of drifting X-ray photogenerated charge carriers as they traverse the photoconductor thickness;

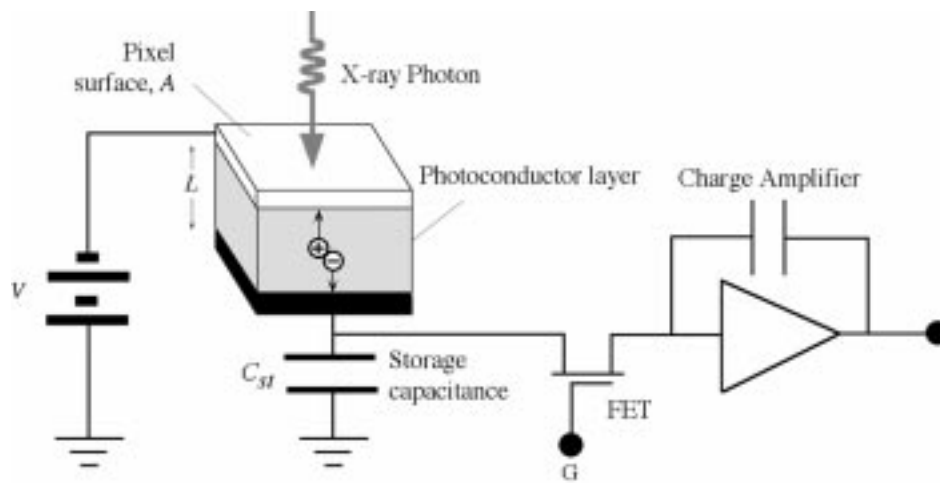


Fig. 5. Schematic diagram representing the equivalent circuit of the photoconductive pixel detector.

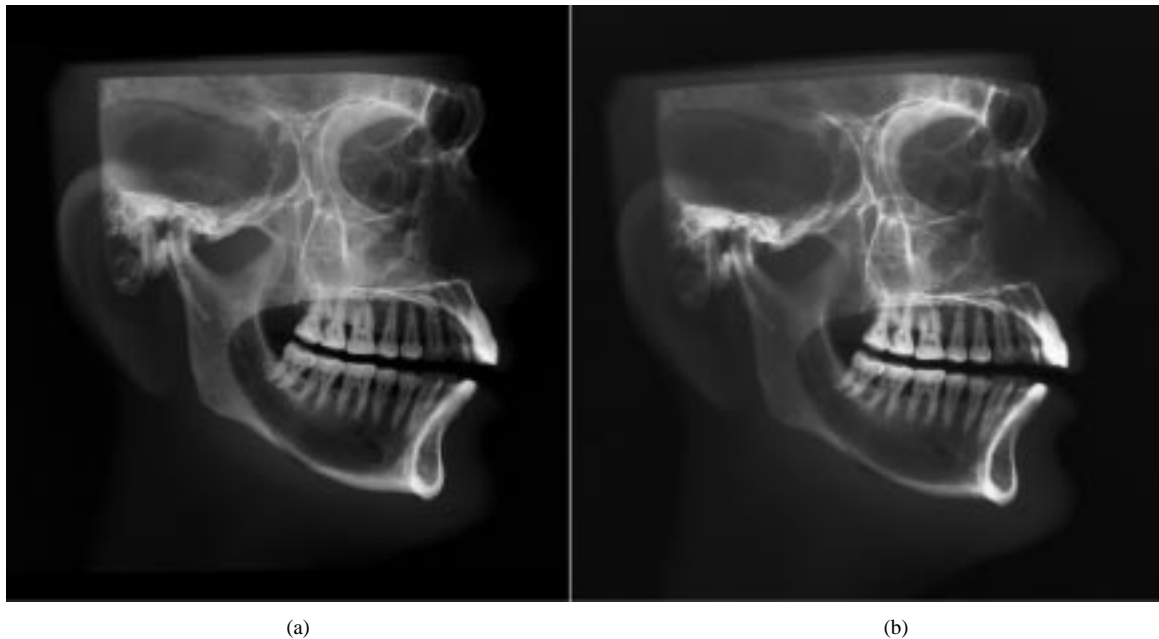


Fig. 6. Comparison of images obtained by (a) an a-Se-based direct-conversion flat-panel X-ray image detector and (b) a screen film.

- 5) lateral spreading due to the internal field arising from injected carriers, i.e., space charge effects that arise as a result of the charge of the injected carriers or, in other words, Coulombic repulsion between the drifting charges of the same sign;
- 6) induced charges in neighboring pixels due to trapped (uncollected) charges in the photoconductor;
- 7) bulk space charge due to trapped carriers perturbing the field which modifies the photogeneration process and changes the charge carrier transport and collection characteristics;
- 8) geometric blurring due to the oblique incidence of X-rays and finite-photoconductor thickness.

These effects are schematically illustrated in Fig. 7. Que and Rowlands found that the range of primary electrons generated by the absorbed X-ray photon and the oblique X-ray incidence effect limits the resolution of the a-Se photocon-

ductor. They were able to conclude that the inherent resolution of the a-Se photoconductor system is far superior to that of the CsI-based columnar phosphor system. Indeed, reported experimental resolution of an a-Se photoconductor with an electrostatic readout system is better than 500 line pairs per millimeter for 16–18 kVp X-rays [10], whereas the physical analysis shows that this could be still higher [9]. The range of the primary electron that is generated by an absorbed photon depends on its energy and the density of the material. This range is typically $\sim 1\text{--}3\ \mu\text{m}$ at 10–30 keV and $\sim 10\text{--}30\ \mu\text{m}$ at 50–100 keV. K-fluorescent X-rays may be released after the interaction of an X-ray photon with the K shell of an atom. The fluorescent X-rays are released isotropically and can be reabsorbed at a point distant from their creation, thus, giving rise to a characteristic type of blurring above the K edge of selenium. Geometrical blurring arises when X-rays are obliquely incident. Since photons are absorbed at different depths, they give a different response at

Table 1
Parameters for Digital X-Ray Imaging Systems. (Data From Rowlands and Yorkston)

| Clinical Task → | Chest radiology | Mammography | Fluoroscopy |
|---------------------------|-----------------|---------------|-----------------|
| Detector size | 35 cm × 43 cm | 18 cm × 24 cm | 25 cm × 25 cm |
| Pixel size | 200 μm × 200 μm | 50 μm × 50 μm | 250 μm × 250 μm |
| Number of pixels | 1750 × 2150 | 3600 × 4800 | 1000 × 1000 |
| Readout time | ~ 1 s | ~ 1 s | 1/30 s |
| X-ray spectrum | 120 kVp | 30 kVp | 70 kVp |
| Mean exposure | 300 μR | 12 mR | 1 μR |
| Exposure range | 30 - 3000 μR | 0.6 – 240 mR | 0.1 - 10 μR |
| Radiation (quantum) noise | 6 μR | 60 μR | 0.1 μR |

the collecting pixels depending on the depth of absorption. For an a-Se photoconductor of thickness 200–1000 μm and for the largest angle of incidence of the order of 15°, the blurring can be of the order of 50–250 μm (a significant amount compared to pixel size). However, this is also highly dependent on the absorption coefficient that is energy dependent.

III. IDEAL X-RAY PHOTOCONDUCTORS

The flat-panel X-ray image detectors, described in Section I, with an a-Se photoconductor has been demonstrated to provide excellent images, as shown in Fig. 6. A-Se may not be the only choice. It is, therefore, instructive to identify what constitutes a nearly perfect X-ray photoconductor to motivate a search for improved performance or better materials. Ideally, the photoconductive layer should possess the following material properties.

- 1) Nearly all the incident X-ray radiation should be absorbed within a practical photoconductor thickness to avoid unnecessary patient exposure. This means that over the energy range of interest, the absorption coefficient α due to the photoelectric effect must be large; the X-ray absorption depth δ must be substantially less than the device layer thickness L .
- 2) The photoconductor should have a high intrinsic X-ray sensitivity, i.e., it must be able to generate as many collectable (free) EHPs as possible per unit of absorbed radiation. This means the amount of radiation energy required, denoted as W_{\pm} , to create a single free electron and hole pair must be low because the free (or collectable) charge ΔQ generated from an incident and absorbed radiation of energy ΔE is simply $e\Delta E/W_{\pm}$. Since, for many material systems, W_{\pm} is proportional to the bandgap E_g , this requirement needs a small bandgap photoconductor.
- 3) The dark current should be negligibly small. This means the contacts to the photoconductor should be noninjecting and the rate of thermal generation of carriers from various defects or states in the bandgap should be negligibly small (i.e., dark conductivity is practically zero). Small dark conductivity generally requires a wide bandgap semiconductor that conflicts with Condition 2 above. The dark current should preferably not exceed ~ 10 – 100 pA cm⁻², depending on the clinical application.
- 4) There should be no bulk recombination of electrons and holes as they drift to the collection electrodes; EHPs are generated in the bulk of the photoconductor. Bulk recombination is proportional to both the concentration of holes and electrons and typically it is negligible provided the instantaneous X-ray exposure is not too high.
- 5) There should be no deep trapping of EHPs, which means that, for both electrons and holes, the schubweg $\mu\tau F \gg L$, where μ is the drift mobility, τ is the deep trapping time (lifetime), F is the electric field, and L is the photoconductor layer thickness. The schubweg is the distance a carrier drifts before it is trapped and, thereby, becomes unavailable for conduction and collection by the external circuit.
- 6) The longest carrier transit time, which depends on the smallest drift mobility, must be shorter than the access time of the pixel and interframe time in fluoroscopy.
- 7) The above should not change or deteriorate with time and as a consequence of repeated exposure to X-rays, i.e., X-ray fatigue and X-ray damage should be negligible.
- 8) The photoconductor should be easily coated onto the AMA panel, e.g., by conventional vacuum techniques without raising the temperature of the AMA to dam-

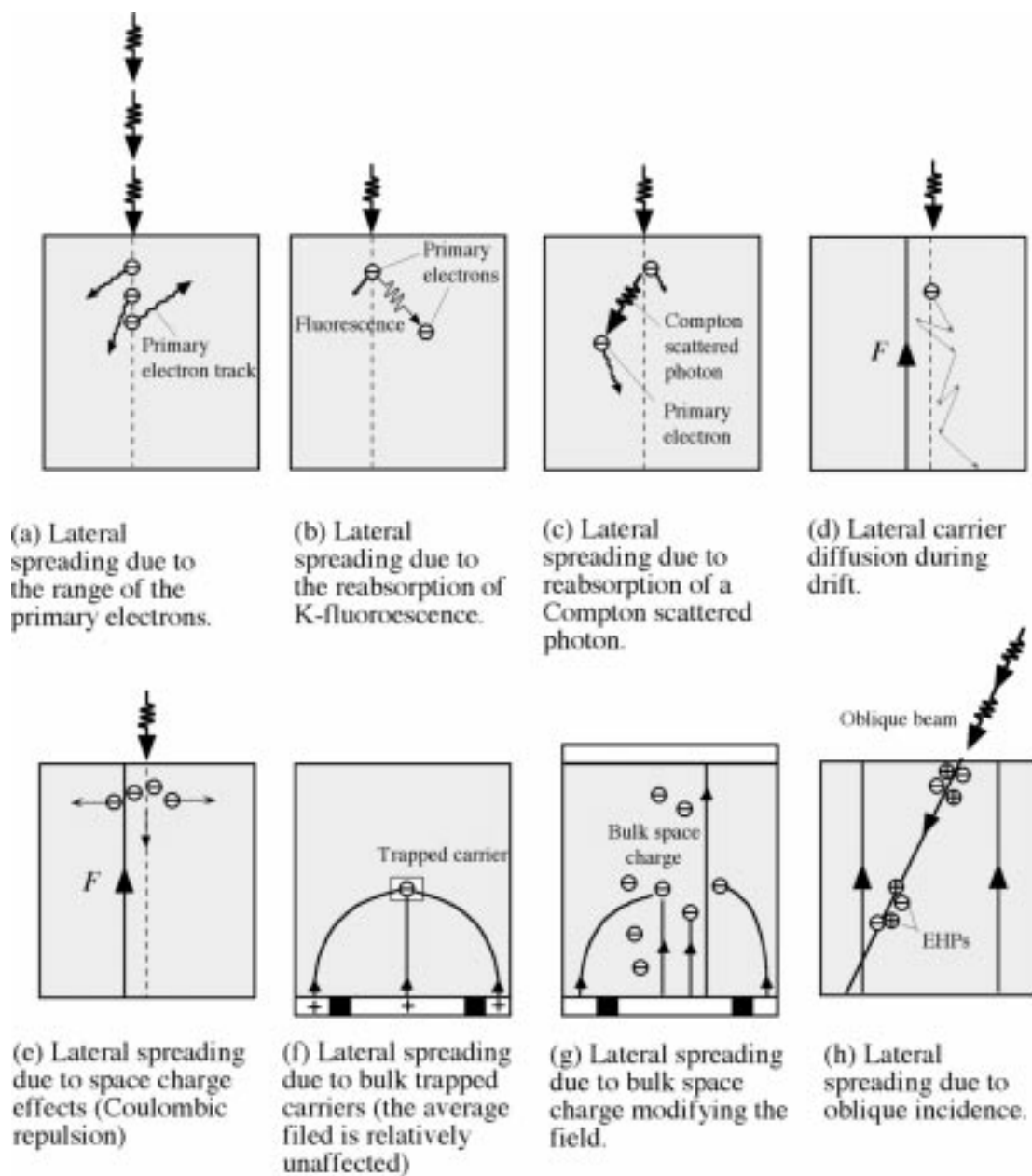


Fig. 7. Various mechanisms that can lead to the broadening of the image and, hence, a loss of resolution in a photoconductor-based X-ray imaging system.

aging levels (e.g., $\sim 300^\circ\text{C}$ for a-Si:H panels). Special processes are generally more expensive. The photoconductor should be coatable on a large area substrate. A large-area detector is essential in radiography since the lack of a practical means to focus X-rays necessitates a shadow X-ray image that is larger than the body part to be imaged.

IV. X-RAY ABSORPTION AND QUANTUM EFFICIENCY

It is highly desirable in medical imaging for the photoconductor to absorb as much of the incident radiation energy as possible to minimize patient exposure. The fraction of incident photons in the beam that are attenuated by the photo-

conductor depends on the linear attenuation coefficient α of the photoconductor material and its thickness L and is given by

$$A_Q = \text{attenuated fraction} = [1 - \exp(-\alpha L)] \quad (1)$$

where $\alpha(E, Z, d)$ is the linear attenuation coefficient of the material and is a function of energy E , atomic number Z , and density d of the material. A_Q is called the quantum efficiency because it describes the efficiency with which the medium attenuates photons. The reciprocal of α is the attenuation depth δ , where the beam has been attenuated by 63%. If each photon has an energy E , neglecting secondary interactions, the actual energy absorbed per photon is given by

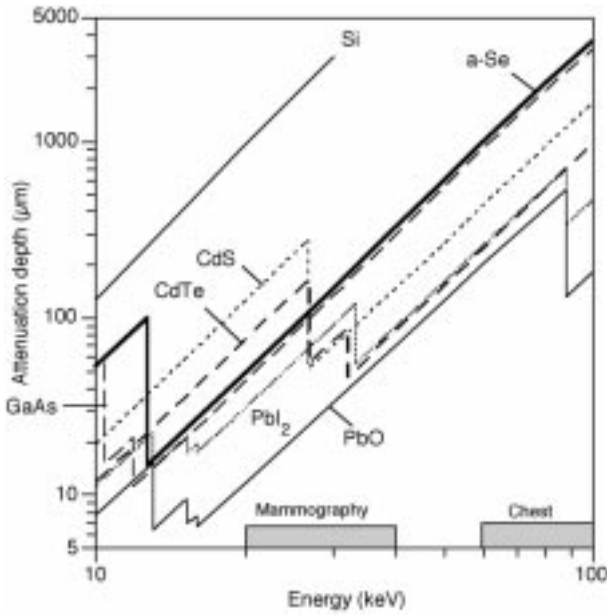


Fig. 8. Attenuation depth (μm) versus photon energy (keV) for various materials. Attenuation coefficients calculated by the authors using elemental mass attenuation coefficients and the density of each material taking into account the chemical formula. Data obtained from Hubbel and Seltzer, 1997, <http://physics.nist.gov/PhysRefData/XrayMassCoef/cover.html>. An extensive list of references are available at this site.

$E(\alpha_{en}/\alpha)$, where α_{en} is the energy absorption coefficient. The actual energy deposited into the photoconductor per unit area is then given by

$$E_{\text{absorbed}} = \int_0^{E_{\text{max}}} \Phi(E) E \frac{\alpha_{en}(E)}{\alpha(E)} (1 - \exp[-\alpha(E)L]) dE \quad (2)$$

where $\Phi(E)$ is the photon fluence per unit energy, i.e., number of photons arriving per unit area per unit energy, which is the energy spectrum of the X-ray beam. The energy absorbed by a given photoconductor material can be maximized by making the detector thickness L several times the attenuation depth δ .

Fig. 8 shows the energy dependence of the attenuation depth δ for a selection of photoconductors. The initial interaction of an X-ray photon with an atom of the material leads to the emission of an energetic electron from an inner core, such as the K-shell, into the conduction band. This is the photoelectric effect and, in the plots of δ against E curves in Fig. 8, it corresponds to the sharp vertical edges. In between the edges, as the energy increases, the attenuation depth increases as E^n , where $n \approx 3$. The absorption depth decreases with the atomic number Z of the material, as $\delta \propto Z^{-n}$, where $n \sim 3-4$. The primary reason for inexpensive organic semiconductors and a-Si:H being excluded as X-ray photoconductors in medical imaging is their low Z . Comparison of photoconductor materials involves the identification and matching of their K and L edges to their potential use such as mammography or chest radiology.

Table 2 summarizes the absorption depths for various candidate X-ray photoconductor materials at photon energy of 20 keV (mammographic X-ray) and 60 keV (chest X-ray). The minimization of dosage requires the absorption depth such that the most of the radiation is absorbed within the thickness L or $\delta < L$. This means that L depends on the E and, hence, the particular imaging application and the locations of the K and L edges of the X-ray photoconductor material. The K edge of a-Se is ~ 12.7 keV, making it particularly useful for mammographic applications, where $E \sim 20$ keV. For mammography, $L = 2\delta \sim 100 \mu\text{m}$. For chest radiology with mean photon energy of 60 keV, $L \sim 2000 \mu\text{m}$. For comparison, the corresponding thicknesses for a HgI_2 detector are about 60 and 540 μm , respectively. However, as L is increased, there is an increased probability that the freed charges will be trapped as they drift across greater distances to reach the electrodes, i.e., the sensitivity may become schubweg-limited, as discussed in Section V.

V. X-RAY SENSITIVITY

The total collectable charge ΔQ generated from an absorbed photon of energy ΔE is $\Delta E/W_{\pm}$ and should be maximized to maintain a signal size larger than system noise. This means that the amount of radiation energy W_{\pm} required to create a single EHP must be as low as possible. Thus, any candidate material for a direct-conversion X-ray imaging application must have an excellent X-ray photoconductivity. Experiments to determine the charge generated by X-rays have shown that it depends on the absorbed radiation energy, i.e., $\Delta Q \propto \Delta E$.

The creation of EHPs by an incident energetic particle or an X-ray photon first involves the generation of an energetic primary electron by ionizing an inner core shell, e.g., the K-shell. As this energetic photoelectron travels in the solid, it causes ionization along its track and hence the creation of many EHPs. For most semiconductors the energy W_{\pm} required to create an EHP has been shown to depend on the energy bandgap E_g via Klein's rule [11] $W_{\pm} \approx 2.8E_g + E_{\text{phonon}}$. The phonon energy term E_{phonon} is expected to be small (< 0.5 eV) so that typically W_{\pm} is close to $2.8E_g$. Further, in crystalline semiconductors, W_{\pm} is field independent and well defined. This W_{\pm} is so well defined in high-purity Si and Ge crystals that they are used in spectrometers to measure the energy of X-rays [12]. Fig. 9 shows the correlation between the EHP creation energy W_{\pm} and the bandgap energy E_g , where the straight line represents a $W_{\pm} \approx 2.8E_g + 0.5$ behavior (the phonon term was taken roughly as ~ 0.5 eV; [13]). Many semiconductors lie on this straight line. In contrast there are also materials such as stabilized a-Se that exhibit a field dependent W_{\pm} . The origin of this field dependence has not been conclusively identified. Fig. 10 shows the field dependence of W_{\pm} in a-Se for monoenergetic X-rays from about 40 to 140 keV [14].

Que and Rowlands [15] argued that if the conservation of k rule is relaxed for amorphous semiconductors, then instead of Klein's rule, the EHP creation energy should be $\sim 2.2E_g + E_{\text{phonon}}$. The field dependence of W_{\pm} in a-Se

Table 2

Densities, Attenuation Depths ($\delta = 1/\alpha$) at a Photon Energy of 20 and 60 keV, and Bandgap Energies (E_g) of Potential X-Ray Photoconductor Materials, at $F = 10$ V/ μ m and b at $F = 30$ V/ μ m

| Photoconductor | TlBr | PbO | PbI ₂ | HgI ₂ | Ge | GaAs | α -Se | GaSe | ZnTe | CdS | CdSe | CdTe |
|-------------------------------|------|------|------------------|------------------|------|------|--------------|------|------|------|------|------|
| Density (g cm ⁻³) | 7.5 | 9.8 | 6.1 | 6.3 | 5.32 | 5.31 | 4.3 | 4.6 | 6.34 | 4.82 | 5.81 | 6.06 |
| δ (μ m) at 20 keV | 18 | 11.8 | 28 | 32 | 44 | 44 | 48 | 49 | 58 | 127 | 56 | 77 |
| δ (μ m) at 60 keV | 317 | 218 | 259 | 252 | 929 | 926 | 976 | 1026 | 300 | 439 | 385 | 250 |
| E_g (eV) | 2.7 | 1.9 | 2.3 | 2.1 | 0.7 | 1.42 | 2.3 | 2.0 | 2.26 | 2.3 | 1.8 | 1.5 |
| W_{\pm} (eV) | 6.5 | 8-20 | 5 | 4.1 | 1.5 | 6.3 | 45a, 20b | 6.3 | 7 | 7.2 | 5 | 4.65 |

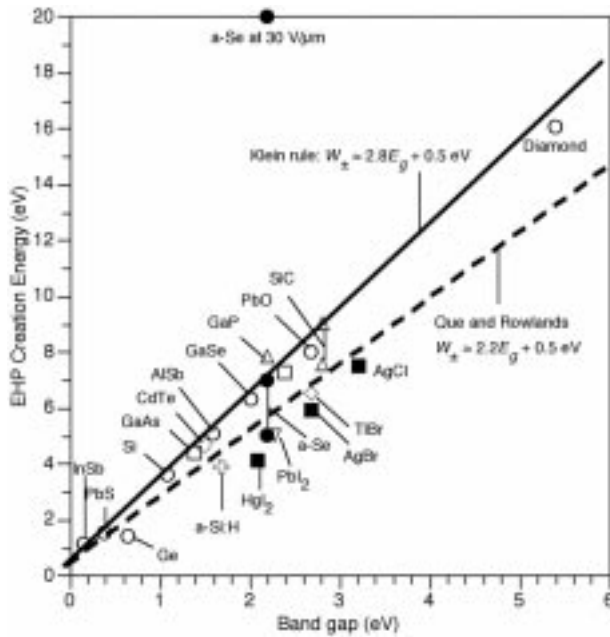


Fig. 9. EHP creation energy versus energy bandgap E_g for various materials.

may arises from the recombination mechanism operating for the EHPs generated by the primary electron. The lowest or saturated W_{\pm} , denoted as W_{\pm}^0 , at the highest fields should be $2.2E_g + E_{\text{phonon}}$. With $E_g \approx 2.2$ eV for a-Se, we would expect $W_{\pm}^0 \approx 5.3$ eV. The situation for a-Se as in the case for other low mobility solids has proven to be difficult to understand. The measured W_{\pm} shows a strong field dependence, as shown in Fig. 10. The saturated W_{\pm} , i.e., W_{\pm}^0 (or the lowest W_{\pm}), has been only estimated by extrapolation to high fields, but seems to be about 6–10 eV, as indicated in Fig. 10. In addition, the apparent EHP creation energy W_{\pm} has been observed to decrease with the photon energy [14], [16], [17], as apparent in Fig. 10. However, the strength of the dependence of W_{\pm} on photon energy has not been fully explained in the literature and is currently a topical research area.

There are various reasons for the field dependence of the EHP creation energy as discussed by the present authors [18].

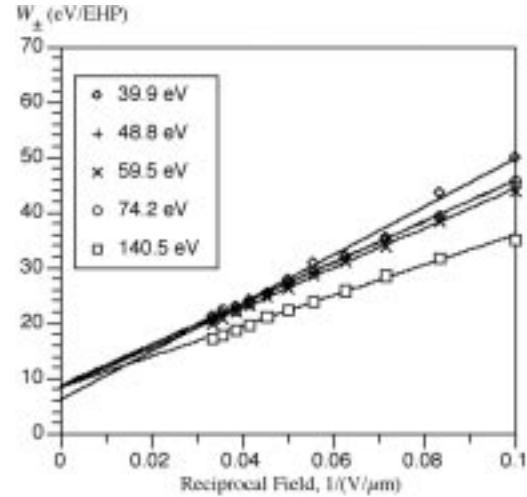


Fig. 10. W_{\pm} versus reciprocal field for various X-ray photon energies as measured using pulse height spectroscopy and radiation obtained from radioactive elements. 39.9 keV fluorescence from Sm, 48.8 keV fluorescence from Er (both excited by 59.9-keV radiation from Am-241), 59.5 keV from AM-241, and 140 keV from Tc-99 m. 74.1-keV fluorescence from Pb excited by 140 keV from Tc-99 m [14].

The primary electron generates many EHPs, but only a certain fraction of these are collected because some are lost by recombination and some become trapped as they drift across the photoconductor. The reduction in the X-ray sensitivity, which is an apparently large W_{\pm} , due to some of the carriers being trapped while drifting to the collection electrodes represents a schubweg-limited sensitivity and is discussed later. Assuming that there are almost no carriers lost due to trapping, as will be the case for a very high quality photoconductor material, then the recombination losses can be attributed to three sources.

- 1) Simple bulk recombination or bimolecular recombination between drifting electrons and holes occurs. The recombination rate is proportional to the product of the hole and electron concentrations so that the collected charge does not increase linearly with the intensity of the radiation. In fact, it depends on the square root of

Table 3

Typical Charge Carrier Schubwegs and Dark Currents in Selected Potential X-Ray Photoconductors

| | a-Se | PbI ₂ | HgI ₂ | TlBr | PbO |
|--|------------------|--|---|-------|-----------------------------------|
| 2δ for 20 keV (mm) | 0.10 | 0.056 | 0.064 | 0.036 | 0.024 |
| 2δ for 60 keV (mm) | 2 | 0.52 | 0.50 | 0.63 | 0.44 |
| F (V/ μ m) | 10; 30 | 0.5 | 0.5 | 1 | 4 |
| $s_h = \mu_h \tau_h F$ (mm) | 6 - 60; 18 - 180 | 0.1 | 0.05 | 0.15 | ? |
| $s_e = \mu_e \tau_e F$ (mm) | 0.3 - 3; 0.9 - 9 | 0.004 | 0.5 | 1.6 | ? |
| I_{dark} (nA cm ⁻²) | 0.01 | 2 at 0.5 V μ m ⁻¹ ; 8 at 2 V μ m ⁻¹ | 1 - 4 at 0.5 V μ m ⁻¹ | | 1 at 4 V μ m ⁻¹ |

the intensity. Experiments, however, show that ΔQ increases linearly with intensity [19], which rules out this type of recombination.

- 2) Geminate recombination in which the electron and hole twin generated at the same time are attracted to each other by their mutual Coulombic force and recombine; hence, the term geminate recombination.
- 3) Recombination loss mechanism or columnar recombination involves the recombination of nongeminate electrons and holes in the columnar track of a primary electron, i.e., bimolecular recombination within a track. (Jaff  [20] first treated the theory of columnar recombination in 1913 by considering the effect of an applied field as a perturbation on the diffusion and recombination of ions in a cylindrical volume. The ions can either recombine or escape recombination and thereby leave the column.) Experiments carried out on a-Se over the diagnostic energy range tend to support the columnar recombination model.

Direct metal to a-Se contacts used in the early work limited the maximum field strength to ~ 10 V μ m⁻¹, where the value of W_{\pm} is 40–50 eV. The recent development of improved blocking layers keeps the dark current at a low value, permitting the electric field to be increased [6]. A significant increase in signal should, therefore, be possible in future devices, utilizing these new blocking contacts. A field of 30–80 V μ m⁻¹ is high enough to increase the signal, but low enough to avoid the potential complications of the avalanche region (i.e., absorption depth dependent gain). The current theoretical and experimental interest in characterizing and understanding the EHP creation energy in amorphous semiconductors is expected to continue, given the importance of this class of materials in large area X-ray photoconductor applications.

It is important to emphasize that the intrinsic W_{\pm} as derived in (5) refers to the number of free EHP that are cre-

ated and collected per incident radiation energy, assuming that none of the charge carriers are captured by deep traps or disappear by recombination. If μ_e is the drift mobility of an electron drifting in the presence of an applied field F and τ_e is its deep trapping time (lifetime), then the electron traverses a distance $s_e = \mu_e \tau_e F$ before it is captured. This distance is called the schubweg. For holes, $s_h = \mu_h \tau_h F$, where μ_h is the hole drift mobility and τ_h is the hole lifetime. If the schubweg is much longer than the detector thickness L , then all the X-ray-generated carriers will be collected and the sensitivity will be limited by W_{\pm} alone. If one or both types of carries have a schubweg less than L , then the sensitivity will be reduced by the loss of carriers to deep traps which become uncollected. The relationship between the collected charge ΔQ and the photoconductor properties $W_{\pm}(E, F)$ and carrier schubwegs has been derived in the literature with special attention to a-Se [21]. At sufficiently high fields, the schubweg can be made to exceed the detector thickness in which case the collected charge ΔQ becomes limited only by W_{\pm} . The room-temperature hole mobility μ_h in a-Se is remarkably reproducible with a value of about $0.12 \text{ cm}^2 \cdot \text{V}^{-1} \cdot \text{s}^{-1}$. In contrast, the electron drift mobility is $\sim 0.003\text{--}0.006 \text{ cm}^2 \cdot \text{V}^{-1} \cdot \text{s}^{-1}$. The value of μ_e decreases rapidly with As addition so that small As concentration variations can affect the mobility. The charge carrier lifetimes, on the other hand, vary substantially between different samples and have been observed to depend on factors such as the source of a-Se, impurities, and the preparation method. For example, the hole lifetime drops sharply with decreasing substrate temperature, whereas the electron lifetime does not seem to depend on the substrate temperature. The electron lifetime is particularly sensitive to impurities in the a-Se source material. Typical range of lifetimes reported have been 50–500 μ s for holes and 100–1000 μ s for electrons. The corresponding schubwegs are listed in Table 3. For a typical a-Se mammographic detector thickness of 200

μm operating at $F = 10 \text{ V}/\mu\text{m}$, the carrier schubwegs have essentially no effect on the X-ray sensitivity, which is limited primarily by W_{\pm} . On the other hand, at higher X-ray energies (60 keV), the detector thickness has to be about 1 mm or greater to maximize A_Q and the electron schubweg significantly impacts sensitivity.

Recently, there has been active research to find potential candidate X-ray photoconductors to replace a-Se in flat-panel sensors. The reason is that despite its various distinctly favorable qualities, a-Se has three identifiable problems.

- 1) The very high voltage needed to activate the a-Se layer could, under fault conditions, possibly damage the a-Se active-matrix array.
- 2) The lower than ideal W_{\pm} .
- 3) The relatively low Z resulting in the requirements for very thick layers to maintain high quantum efficiency.

Table 2 lists the EHP creation energies for a selection of photoconductor materials.

Single-crystal PbI_2 was first investigated for nuclear radiation detectors. More recently, thin layers have been deposited onto active-matrix arrays to form an X-ray imaging system [32]. It shows an adequate schubweg provided that relatively high biasing fields ($2 \text{ V}/\mu\text{m}^{-1}$) are used. PbO has also been used as an imaging photoconductor for some time. The first application (in 1954) was in an optical vidicon [22] and a large-area X-ray vidicon was made in 1956 [23]. The vidicon tube had a diameter of 8 in and had a $150\text{-}\mu\text{m}$ -thick layer of PbO in a p-i-n structure. The p and n regions were obtained by doping the PbO ; the intrinsic region was obtained by making the PbO porous. Values of W_{\pm} , i.e., $\sim 8 \text{ eV}$, have been reported for crystalline PbO , but higher values for evaporated layers [24]. It is difficult to manufacture because it reacts immediately with ambient air, causing both its dark resistance and its X-ray sensitivity to decrease. A more serious problem with thick layers is the degradation with use characterized by: image persistence, nonuniformity, white spots, and decreasing sensitivity [25]. It has also been used for the construction of prototype flat-panel imaging systems [24]. TlBr [26] is a crystalline semiconductor with high ionic conductivity that gives rise to a large dark current. However, sufficiently good films have been made, which have been used as the photoconductor for large-area vidicons where it is cooled with a Peltier cooler [27] to reduce the ionic current to negligible levels. There is a host of other materials under investigation as potential photoconductors for medical X-ray imaging including CdTe [28], CdZnTe , and HgI_2 [29], [30]. Indeed, recent research on HgI_2 layers has shown that this photoconductor can be deposited to exhibit both low dark currents and acceptable charge carrier schubwegs at reasonable applied fields. Good images have been demonstrated using HgI_2 as a photoconductor on an AMA. In the coming years, it is likely that many of these will be combined with active-matrix arrays to investigate their potential for diagnostic radiology. New engineered materials known as nanocomposite organic photoconductors [31], consisting of nanoparticles of heavy metals in an organic photoconductor matrix, also hold promise.

Table 3 summarizes typical charge carrier schubwegs for selected potential X-ray photoconductors. The table also includes the dark current inasmuch as in some cases, such as PbI_2 , acceptable schubwegs require fields that lead to undesirably large dark currents.

The large-area coating requirement over areas typically $30 \text{ cm} \times 30 \text{ cm}$ or greater rules out the use of X-ray sensitive crystalline semiconductors, which are difficult to grow in such large areas. Although various X-ray photoconductor materials are currently in commercial use, most of their device applications involve small areas, typically less than $\sim 1 \text{ cm}^2$. These X-ray photoconductors are either single crystal or polycrystalline in form. Both CdSe and PbO evaporated layers are used in 1-in diameter X-ray vidicons. PbI_2 polycrystalline layers have an unacceptable dark current even under a small applied bias, which results in a schubweg-limited sensitivity [32]–[34]. Recent experiments using PbI_2 and HgI_2 polycrystalline X-ray photoconductive layers on AMA have shown encouraging results [35], [36]. Although polycrystalline semiconductors such as $\text{Zn}_x\text{Cd}_{1-x}\text{Te}$, PbI_2 , and HgI_2 have the feasibility to be prepared in large areas, their main drawback is the adverse affect of grain boundaries in limiting charge transport and, further, the high substrate and annealing temperatures required to optimize the semiconductor properties, which may be incompatible with the a-Si AMA substrates.

VI. NOISE

The noise in the number of X-rays Q or signal incident on the detector is given by the Poisson fluctuations in Q . The X-ray absorption noise N is then

$$N = Q^{0.5}. \quad (3)$$

The square of the signal-to-noise ratio (SNR) $_{\text{in}}^2$ is

$$\text{SNR}_{\text{in}}^2 = \frac{Q^2}{Q} = Q. \quad (4)$$

The SNR of monoenergetic X-rays totally absorbed in an ideal detector with quantum efficiency A_Q is, therefore,

$$\text{SNR}_{\text{out}}^2 = \frac{(A_Q^2 Q^2)}{(A_Q Q)} = A_Q Q. \quad (5)$$

Substituting (4) into (5) so as to eliminate Q we obtain

$$A_Q = \frac{\text{SNR}_{\text{out}}^2}{\text{SNR}_{\text{in}}^2}. \quad (6)$$

There are many assumptions inherent in this derivation, including: 1) the X-rays are monoenergetic; 2) the X-rays are totally absorbed; and 3) the response to a given amount of absorbed energy is always the same. In reality, in medical imaging a broad spectrum of X-ray energies from an X-ray tube leads to variability in the energy deposited per X-ray. When an X-ray is absorbed, there is a high probability that a K-fluorescence X-ray may be emitted reducing the amount of energy absorbed in a random manner. Finally, the X-ray to

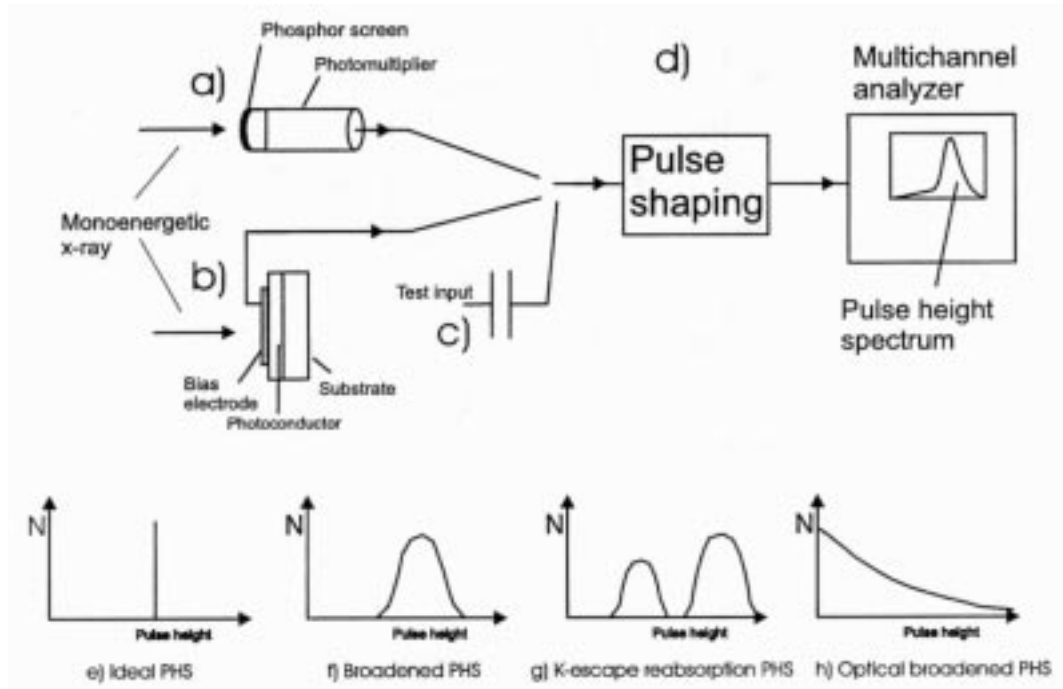


Fig. 11. Experimental methods to measure PHS for (a) phosphor layers, (b) photoconductors, (c) test input for calibration of system in terms of charge, and (d) electronics to shape pulses from individual X-ray absorption to have a height proportional to charge deposited per X-ray. (e)–(h) Example PHS that may be observed and the corresponding value of the Swank information factor A_s . (e) Ideally, a single delta function giving Swank factor $A_s = 1$. (f) Single peak broadened by statistical processes in the screen or phosphor layer $A_s \sim 0.95$. (g) Extra (lower energy) peak caused by K-fluorescence escape giving $A_s \sim 0.75$. (h) Extreme broadening of peak to the extent that it is exponential, which can arise because of absorptive dye in phosphor layer or its backing layer giving $A_s \sim 0.5$.

the ionization process and charge carrier conversion energy W_{\pm} has its own fluctuations due to the ionization process and charge carrier recombination and trapping. These fluctuations are caused by the statistical nature of the competing mechanisms that occur as the X-ray deposits energy in the medium. These effects of noise are known as gain-fluctuation noise. The first discussion of gain-fluctuation noise and estimates of its magnitude, in the context of X-ray detection with phosphors, was given by Swank [37].

The gain-fluctuation noise is experimentally determined using the pulse height spectrum (PHS) obtained using monoenergetic X-ray sources, as shown in Fig. 11 for a photoconductor. Monoenergetic X-rays are incident on the detector, one at a time. For each absorbed X-ray photon incident, a quantity of charge is released by the photoconductor. The amount of released charge in the photoconductor is measured by using a pulse-shaping circuit, which integrates the X-ray charge into a pulse whose height is proportional to the integrated charge. The multichannel analyzer (see Fig. 11) then digitizes the pulse height and increments a counter corresponding to that height. This creates a histogram called a PHS. This can be interpreted and, if necessary, calibrated using a charge terminator, as shown in Fig. 11, in terms of charge or deposited X-ray energy.

Prototypical pulse height spectra are shown in Fig. 11(e) to (h). Fig. 11(e) is the ideal spectrum—all X-rays produce equal amounts of charge, resulting in a delta function. As shown in the caption, this has a value of the Swank factor

$A_s = 1$. Other possible shapes due to statistical broadening or K-fluorescence escape will have the form shown and the corresponding approximate value of A_s is given in the caption to Fig. 11. Such measurements and related theoretical estimates have been performed for layers of stabilized a-Se [38], [39]. The noise due to both quantum absorption inefficiency and gain fluctuations can be combined to create the zero spatial frequency detective quantum efficiency DQE(0)

$$\text{DQE}(0) = A_Q A_S \quad (7)$$

where A_S is the correction due to gain fluctuation noise and can be expressed in terms of $i = 0, i = 1, i = 2$, the i th moments of the PHS, i.e., the histogram of $N(\epsilon)$ plotted against ϵ , where ϵ is the energy

$$M_i = \sum N(\epsilon) \epsilon^i \quad (8)$$

as a combination of the zeroth, first, and second moments

$$A_s = \frac{M_1^2}{(M_0 M_2)}. \quad (9)$$

Representative calculated values for the magnitude of the Swank factor A_S are plotted in Fig. 12 for two representative photoconductors. These calculations include only the broadening effects of the intrinsic X-ray phenomena, not recombination or trapping. They, thus, represent an upper limit on A_S . The energy of the incident X-ray is important since above the K edge of the material, K-fluorescence

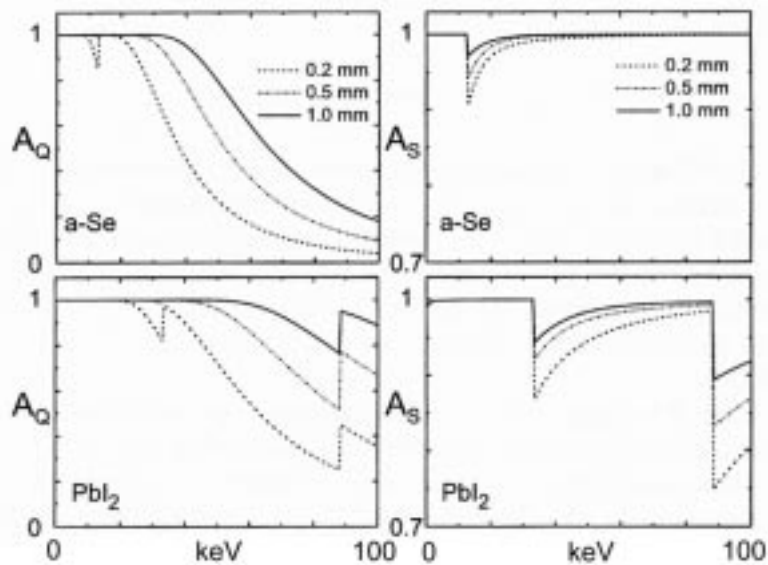


Fig. 12. Quantum efficiencies A_Q and gain fluctuation (Swank) factors A_S for two representative photoconductors, a-Se and PbI_2 . Curves are calculated using the photoelectric attenuation coefficient only. (Graphs courtesy of D. Hunt.)

escape can significantly affect the distribution of measured signals and reduce the Swank factor, thus, increasing Swank noise. Higher Z materials with K edges in the range of energies present in a diagnostic X-ray beam will exhibit more image degradation due to this mechanism than lower Z elements with K edge at lower energies. However, changes in the absorption coefficient across the K edge can make higher Z materials less sensitive, on average, to the lower energy scattered radiation produced in the patient [40]. This scattered radiation is an additional source of noise that may reduce the quality of the final image.

VII. MEDICAL APPLICATIONS

The medical applications for which flat-panel detectors are being developed and the new opportunities made possible with this technology will be discussed in the context of the procedures currently used in clinical practice. All clinical applications will benefit from the following general features of flat-panel detectors, including: compactness, ability to be read out immediately after radiation exposure to verify patient position and appropriate image exposure, ability to permit digital storage and communication within the hospital and beyond, facilitation of computer-aided diagnosis and “second opinions,” and perhaps, most importantly, the possibility of improving image quality without increasing patient X-ray exposure due to their enhanced detective quantum efficiency. Another less recognized benefit is their inherent computer control and that the majority of modern X-ray machines are microprocessor controlled. The complete synchronization of the delivery of the X-ray exposure, the acquisition and readout of the image, and the movement of the X-ray tube and other mechanical devices such as filter holders as well as computer control of the X-ray energy is, thus, possible. Complex imaging procedures, such as dual energy and tomographic data acquisition, improve the busy clinical en-

vironment. The following will describe the requirements of important clinical imaging tasks and the improvements possible by digital X-ray imaging and flat-panel X-ray detectors.

A. Chest Radiography

Flat-panel active-matrix X-ray imagers have been configured for chest imaging. The foremost requirements are (see Table 1) a very large field of view, a reasonably high spatial resolution (100–200- μm pixels), and a very large dynamic range to accommodate the different penetration of the lungs and mediastinum. Digital image processing can be used to equalize the appearance of the image and, thus, lower X-ray beam will be used in the future.

B. Mammography

Mammography is the only projection X-ray imaging modality that attempts to visualize soft tissue contrast and, thus, requires very highly absorbing beams [41]. Film/screen is the current gold standard, but it has a small dynamic range. Therefore, extreme of breast compression to equalize the X-ray path length is needed so that the whole breast can be visualized. Digital mammography is still undergoing development [42], but has potential advantages of increased dynamic range, less breast compression, and the ability to visualize dense breasts. The challenge is to make pixels small enough at an affordable cost. While 100- μm pixels may not be quite small enough, 50 μm will be more than adequate. The intrinsically high resolution of a-Se combined with the relative simplicity of the AMA design used for direct conversion suggests that this may be an ideal approach for mammography [43].

C. Fluoroscopy

Perhaps the most demanding potential application for flat-panel imaging systems is in fluoroscopy. Very high

patient doses often result from lengthy interventional fluoroscopic procedures. During these procedures, low radiation exposure rates must be used to reduce the total exposure to the patient. This sets a stringent limit on the system performance, since the image quality must still be adequate for visualization of the interventional tools as well as anatomy. Therefore, the imaging system must be X-ray quantum limited, even at extremely low exposure levels, which implies a very low system noise for the AMA. The current technology uses a large vacuum tube device—an X-ray image intensifier. Active-matrix panels are more compact, permit better access to patients, and since a panel is flat, it is largely free from the geometrical distortions characteristic of vacuum tube X-ray image intensifiers. Thus, quantitative image analysis, registration, and clinical comparison of images from other modalities, three-dimensional construction (e.g., cone beam volume computerized tomography), and use in conjunction with magnetic-resonance imaging are facilitated.

VIII. FUTURE

Flat-panel X-ray detectors are still relatively new. Many advances in system design and improvements in system performance can be expected. As fabrication techniques and device yields improve, more sophisticated switching structures with reduced coupling capacitance, lower leakage currents, smaller physical area, and more robust operating characteristics will continue to be developed. These advances will improve the imaging performance of AMAs until the dominant factor becomes the properties of the X-ray detection medium, even for the most demanding low signal level and high-resolution applications such as fluoroscopy and mammography.

The investigation of large area flat-panel sensors presents a large variety of previously unexplored problems in detector physics. How they may be resolved has been discussed. It is to be expected that at the end of this development, an essentially ideal X-ray imaging detector will be possible. The initial investment has already been high, but over time the image quality and labor saving will justify this investment. In time, mass production will eventually reduce the cost. It is our opinion that flat-panel detectors are poised to be a unifying concept in X-ray medical imaging as they promise to greatly simplify the acquisition, interpretation, storage, and distribution of X-ray images.

REFERENCES

- [1] M. J. Yaffe and J. A. Rowlands, "X-ray detectors for digital radiology," *Phys. Med. Biol.*, vol. 42, no. 1, pp. 1–39, Jan. 1997.
- [2] J. A. Rowlands and J. Yorkston, "Flat panel detectors for digital radiography," in *Handbook of Medical Imaging*, J. Beutel, H. L. Kundel, and R. L. Van Metter, Eds. Washington, DC: SPIE, 2000, vol. 1.
- [3] K. Suzuki, "Flat panel displays using amorphous and monocrystalline semiconductor devices," in *Amorphous and Microcrystalline Semiconductor Devices: Optoelectronic Devices*, J. Kanicki, Ed. Boston, MA: Artech House, 1991, ch. 3.
- [4] L. E. Antonuk, J. Boudry, W. Wang, D. McShan, E. J. Morton, J. Yorkston, and R. A. Street, "Demonstration of megavoltage and diagnostic X-ray imaging with hydrogenated amorphous silicon arrays," *Med. Phys.*, vol. 19, no. 6, pp. 1455–1466, Nov. 1992.
- [5] M. Hoheisel, M. Arques, J. Charbal, C. Chaussant, T. Ducourant, L. Fritsch, G. Hahm, H. Horbaschek, J. Michailos, R. Schulz, M. Soahn, V. Spinnier, and G. Vieux, "Amorphous silicon X-ray detectors," in *Future Directions in Thin Film Science and Technology*, J. M. Marshall, N. Kirov, A. Vavrek, and J. M. Maud, Eds. Singapore: World Scientific, 1997, p. 112.
- [6] B. Polischuk, Z. Shukri, A. Legros, and H. Rougeot, "Selenium direct converter structure for static and dynamic X-ray detection in medical imaging," *Proc. SPIE*, vol. 3336, pp. 494–504, 1998.
- [7] J. A. Rowlands and S. O. Kasap, "New directions in X-ray imaging," in *Proceedings of the Sixth International Symposium on Uses of Selenium and Tellurium*, Y. Palmieri, Ed. Grimbergen, Belgium: STDA, 1998, pp. 25–35.
- [8] B. Polischuk, H. Rougeot, K. Wong, A. Debie, E. Poliquin, M. Hansroul, J. P. Martin, T. Truong, M. Choquette, L. Laperriere, and Z. Shukri, "Direct conversion detector for digital mammography," *Proc. SPIE*, vol. 3659, pp. 417–425, 1999.
- [9] W. Que and J. A. Rowlands, "X-ray imaging using amorphous selenium: Inherent spatial resolution," *Med. Phys.*, vol. 22, no. 4, pp. 365–374, Apr. 1995.
- [10] T. Oguro, I. Kashima, M. Kanno, T. Higashi, T. Uehara, and B. T. Williams, "Ultra high resolution digital xeroradiography for X-ray microscopic detection" (in Japanese), *Med. Image Technol.*, vol. 7, pp. 279–280, 1989.
- [11] C. A. Klein, "Bandgap dependence and related features of radiation ionization energies in semiconductors," *J. Appl. Phys.*, vol. 39, no. 4, pp. 2029–2038, Mar. 1968.
- [12] G. F. Knoll, *Radiation Detection and Measurement*, 3rd ed. New York: Wiley, 2000.
- [13] R. C. Alig and S. Bloom, "Electron-hole pair creation energies in semiconductors," *Phys. Rev. Lett.*, vol. 35, no. 22, pp. 1522–1525, Dec. 1975.
- [14] I. M. Blevis, D. C. Hunt, and J. A. Rowlands, "Measurement of X-ray photogeneration in amorphous selenium," *J. Appl. Phys.*, vol. 85, no. 11, pp. 7958–7962, June 1999.
- [15] W. Que and J. A. Rowlands, "X-ray photogeneration in amorphous selenium: Geminate versus columnar recombination," *Phys. Rev.*, vol. B51, no. 16, pp. 10 500–10 507, Apr. 1995.
- [16] H. Fiedler and F. Laugwitz, "Zur Quantenausbeute elektroradiographischer Selenschichten" (in German), *J. Signal AM*, vol. 9, no. 3, pp. 229–235, 1981.
- [17] D. Mah, J. A. Rowlands, and J. A. Rawlinson, "Sensitivity of amorphous selenium to X-rays from 40 kVp to 18 MV: measurements and implications for portal imaging," *Med. Phys.*, vol. 25, no. 4, pp. 444–456, Apr. 1998.
- [18] S. O. Kasap and J. A. Rowlands, "Review: X-ray photoconductors and stabilized a-Se for direct conversion digital flat panel X-ray image detectors," *J. Mater. Sci. Mater. Electron.*, vol. 11, no. 3, pp. 179–198, Apr. 2000.
- [19] C. Haugen, S. O. Kasap, and J. A. Rowlands, "Charge transport and electron-hole pair creation energy in stabilized a-Se X-ray photoconductors," *J. Phys. D Appl. Phys.*, vol. 32, no. 3, pp. 200–207, Feb. 1999.
- [20] G. Jaffe, "Zur Theorie de Ionisation in Kolonnen," *Ann. der Phys.*, vol. 42, p. 303, 1913.
- [21] S. O. Kasap, "X-ray sensitivity of photoconductors: Application to stabilized a-Se," *J. Phys. D.*, vol. 33, no. 21, pp. 2853–2865, Nov. 2000.
- [22] L. Heijne, P. Schagen, and H. Buining, "An experimental photoconductive camera tube for television," *Philips Tech. Rev.*, vol. 16, p. 23, 1954.
- [23] J. Jacobs and H. Berger, "Large-area photoconductive X-ray pickup-tube performance," *Electr. Eng.*, vol. 75, p. 158, 1956.
- [24] A. Brauers, N. Conrads, G. Frings, U. Schiebel, M. J. Powell, and C. Glasse, "X-ray sensing properties of a lead oxide photoconductor combined with an amorphous silicon TFT array," *Proc. Mater. Res. Soc.*, vol. 507, pp. 321–326, 1998.
- [25] J. Weiss, "Large field cineradiography and image intensification utilising the TVX system," *Radiology*, vol. 76, p. 264, 1961.
- [26] K. S. Shah, J. C. Lund, F. Olschner, L. Moy, and M. R. Squillante, "Thallium bromide radiation detectors," *IEEE Trans. Nucl. Sci.*, pt. 1, vol. 36, p. 199, Feb. 1989.
- [27] D. R. Ouimette, S. Nudelman, and R. Aikens, "A new large area X-ray image sensor," *Proc. SPIE*, vol. 3336, pp. 470–476, 1998.

- [28] S. Adachi, N. Hori, K. Sato, S. Tokuda, T. Sato, K. Uehara, Y. Izumi, H. Nagata, Y. Yoshimura, and S. Yamada, "Experimental evaluation of a-Se and CdTe flat-panel X-ray detectors for digital radiography and fluoroscopy," *Proc. SPIE*, vol. 3977, pp. 38–47, 2000.
- [29] M. R. Squillante, J. Zhang, C. Zhou, P. Bennett, and L. Moy, "New compound semiconductor materials for nuclear detectors," *Proc. Mat. Res. Soc.*, vol. 302, pp. 319–328, 1993.
- [30] W. Bencivelli, E. Bertolucci, U. Bottigli, A. Del Guerra, A. Messineo, W. R. Nelson, P. Randaccio, V. Rosso, P. Rosso, and A. Stefanini, "Evaluation of elemental and compound semiconductors for X-ray digital radiography," *Nucl. Inst. Meth.*, vol. A310, pp. 210–214, 1991.
- [31] Y. Wang and N. Herron, "X-ray photoconductive nanocomposites," *Science*, vol. 273, pp. 632–634, Aug. 1996.
- [32] K. S. Shah, P. Bennett, M. Klugerman, L. P. Moy, and G. Entine, "Lead iodide films for X-ray imaging," *Proc. SPIE*, vol. 3032, pp. 395–404, 1997.
- [33] R. A. Street, K. Shah, S. Ready, R. Abe, P. Bennett, M. Klugerman, and Y. Dmitriyev, "Large area X-ray image sensing using a Pbl₂ photoconductor," *Proc. SPIE*, vol. 3336, pp. 24–32, 1998.
- [34] R. A. Street, J. T. Rahn, S. E. Ready, K. Shah, P. R. Bennett, Y. Dmitriyev, P. Mei, J.-P. Lu, R. B. Apte, J. Ho, K. van Schuylenbergh, F. Lemmi, J. B. Boyce, and P. Nylén, "X-ray imaging using lead iodide as a semiconductor detector," *Proc. SPIE*, vol. 3659, pp. 36–47, 1999.
- [35] R. A. Street, S. E. Ready, J. T. Rahn, M. Mulato, K. Shah, P. R. Bennett, P. Mei, J.-P. Lu, R. B. Apte, J. Ho, K. van Schuylenbergh, F. Lemmi, J. B. Boyce, P. Nylén, M. Schieber, and H. Hermon, "High resolution, direct detection X-ray imagers," *Proc. SPIE*, vol. 3977, pp. 418–428, 2000.
- [36] M. Schieber, H. Hermon, R. A. Street, S. E. Ready, A. Zuck, A. Vilensky, L. Melekhov, R. Shatunovsky, E. Meerson, and Y. Saado, "Radiological X-ray response of polycrystalline mercuric iodide detectors," *Proc. SPIE*, vol. 3977, pp. 48–55, 2000.
- [37] R. K. Swank, "Absorption and noise in X-ray phosphors," *J. Appl. Phys.*, vol. 44, pp. 4199–4203, 1973.
- [38] R. Fahrig, J. A. Rowlands, and M. J. Yaffe, "X-ray imaging using amorphous selenium: Detective quantum efficiency of photoconductive image receptors for digital mammography," *Med. Phys.*, vol. 22, no. 2, pp. 153–160, Feb. 1995.
- [39] I. M. Blevis, D. M. Hunt, and J. A. Rowlands, "X-ray imaging using amorphous selenium: Determination of Swank factor by pulse height spectroscopy," *Med. Phys.*, vol. 25, no. 5, pp. 638–641, May 1998.
- [40] K. L. Yip, B. R. Whiting, T. E. Kocher, D. P. Trauernicht, and R. L. Van Metter, "Understanding the relative sensitivity of radiographic screens to scattered radiation," *Med. Phys.*, vol. 23, no. 10, pp. 1727–1737, Oct. 1996.
- [41] R. Fahrig, J. A. Rowlands, and M. J. Yaffe, "X-ray imaging using amorphous selenium: Optimal spectra for digital mammography," *Med. Phys.*, vol. 23, no. 4, pp. 557–567, Apr. 1996.
- [42] V. Venkatakrishnan, M. Yavuz, L. T. Niklason, B. Opsahl-Ong, S. Han, C. Landberg, R. Nevin, L. Hamberg, and D. B. Kopans, "Experimental and theoretical spectral optimization for digital mammography," *Proc. SPIE*, vol. 3659, pp. 142–149, 1999.
- [43] W. Zhao, J. A. Rowlands, S. Germann, D. F. Waechter, and Z. Huang, "Digital radiology using self-scanned readout of amorphous selenium: Design considerations for mammography," *Proc. SPIE*, vol. 2432, pp. 250–259, 1995.



Safa O. Kasap (Senior Member, IEEE) received the B.S.E.E., M.S., and Ph.D. degrees in electrical engineering from the Imperial College of Science, Technology and Medicine, University of London, U.K., in 1976, 1978, and 1983, respectively, and the D.Sc. in engineering from London University, U.K., in 1996.

He is currently a Professor of Electronic Materials and Devices with the Electrical Engineering Department, University of Saskatchewan, Saskatoon, SK, Canada. He has authored or coauthored more than 100 papers in refereed journals, *Optoelectronics and Photonics: Principles and Practices* (Englewood Cliffs, NJ: Prentice-Hall, 2001), and *Principles of Electronic Materials and Devices, Second Edition* (New York: McGraw-Hill, 2002). His current research interests include amorphous semiconductors, noise in electronic devices, photoconductors, photodetectors, X-ray image detectors, laser-induced transient photoconductivity, and related topics.

Dr. Kasap is a Fellow of the Institution of Electrical Engineers, the Institute of Physics, and the Institute of Materials.



John A. Rowlands received the Ph.D. degree in physics from the University of Leeds, Leeds, U.K., in 1971.

In 1979, he joined the Department of Medical Imaging, University of Toronto, Toronto, ON, Canada, as an Assistant Professor. He has also been with the Department of Medical Biophysics at the same university since 1985, where he became a Full Professor in 1998. His current research interests include advancing the state of the art in medical X-ray detectors and particularly real-time (fluoroscopic) detectors used for cardiac angiography. He pioneered the use of amorphous selenium combined with thin-film active-matrix arrays to make the new generation of flat-panel imagers recently coming into preclinical use.

Dr. Rowlands is a Fellow of the Canadian College of Physicists in Medicine.